ADVANCED MATERIALS
www.advmat.de

www.MaterialsViews.com

Ionic Liquid-Assisted Synthesis of Microporous Carbon Nanosheets for Use in High Rate and Long Cycle Life Supercapacitors

*Zhen-Yu Jin, An-Hui Lu, Yuan-Yuan Xu, Jin-Tao Zhang, and Wen-Cui Li**

Porous carbon materials have received considerable attention owing to their superior physical and chemical properties such as large surface area, tunable pore structure, good electrical conductivity, chemically inert nature and versatile forms.[1,2] These outstanding features make porous carbons ideal candidates for the applications in the renewable energy storage and power output technologies, such as supercapacitors.[3,4] Hitherto, nanostructured porous carbons such as carbon monoliths with hierarchical porosity,[5,6] nanospheres,[7] nanofibers[8,9] or nanotubes,[10] graphene-based materials[11–13] and even graphene[14–18] have been widely explored as electrode materials for supercapacitors.[19] It is generally accepted that no matter which kind of nanostructured carbon is used as the electrode, micropores are crucial sites for strengthening the electric double layer for high capacitance.[20–22] However, microporous-carbon-based supercapacitors are known to suffer from electrode kinetic problems that are related to the limitation of electrolyte ions penetrating the inner pores of an electrode, and improving the rate capacity in such supercapacitors remains an ongoing challenge.[23,24] Therefore, various strategies have been proposed to improve the rate performance of microporous carbon materials. One effective solution is to introduce well-organized mesopores or even larger pores in order to provide a channel for the favorable transport of electrolyte ions.[11,25,26] Unfortunately, due to a screening effect in the mesopores, only some of the ions are effective in contributing to the charge storage process because the others have to balance the counterions in the bulk electrolyte,[27] as a result, the final capacity in terms of energy density needs to be increased to a higher level.[11,28,29] Another practical solution is to increase the accessibility of micropores by improving the wettability of the electrode surface by heteroatom-doping.[30–33] To achieve this, ionic liquids (ILs), known best for their environmentally benign features such as ionicity, stability and heteroatom containing,[34] make themselves attractive in the synthesis of heteroatom-doped carbonaceous materials.[31,35–40] A natural extension of this idea is to integrate the advantages of heteroatom-doping and a thin sheet structure into microporous carbon materials so that one might simultaneously achieve a high capacitance, good rate performance and long cycle life carbon-based supercapacitor. Hence, it is important to establish an efficient synthesis of heteroatom-doped, microporous carbon sheets with controlled thickness, narrow micropore size distribution and high electric conductivity.

In the present work, we report the simple synthesis in an aqueous solution of 2D nitrogen-doped microporous carbon sheets (NMCSs) with precisely controlled thickness, using ionic liquid functionalized graphene oxide (IL-functionalized GO) sheets as a shape-directing agent and a resorcinol/formaldehyde polymer as the carbon precursor. We define this material as microporous carbon sheets rather than graphene or graphene-based sheets because the prepared sheets contain very small amounts of graphene, from 0.26 wt% to 2.72 wt%, and have a graphene inner layer and a carbon coating on both sides. In particular, the obtained carbon sheets show excellent rate capability, a high specific capacitance of 341 F g^{-1} at 5 mV s^{-1}, and good cycle stability over 35000 cycles without any conductive additive.

In the synthesis process, 1-butyl-3-methylimidazolium imidazolide ([BMIM]Im) ionic liquid was selected to stabilize the isolated GO sheets and to functionalize them in an aqueous solution. Resorcinol and formaldehyde were later added to the above solution and polymerization took place immediately. The final pyrolysis step generated 2D NMCSs. To detect the adsorption behavior of [BMIM]Im IL on the surface of GO sheets, we carried out UV absorption spectra for pure GO colloid and IL-functionalized GO colloid. As shown in **Figure 1**, the curve for the GO colloid shows a small broad peak at 210 nm and two tiny shoulders at 230 and 290 nm, characteristic of the π–π^* electron transition in the polyene-type structure of GO sheets and the n-π^* electron transition of C=O bonds.[41,42] In contrast, the absorption peak of the IL-functionalized GO colloid shifts to 195 nm, corresponding to the attachment of ILs to GO sheets by covalent or non-covalent interactions (Figure 1a).[43,44] The dependence of absorbance on the concentration of IL-functionalized GO colloid obeys Beer's law and the correlation coefficient is as high as 0.9998, indicating that the IL-functionalized GO is homogeneously dispersed in the aqueous solution and no concentration-dependent aggregation is observed even after storage for five months (Figure 1b). A direct observation also proves the stability of the IL-functionalized GO colloid (Figure S1).

The morphology of the as-prepared NMCSs was investigated by FE-SEM. As shown in **Figure 2** and Figure S2, one can see that they have a sheet structure. From the fracture edge (Figure 2a, b and d), the carbon sheets seems to be cut into

Z.-Y. Jin, A.-H. Lu, Prof. Y.-Y. Xu, J.-T. Zhang, Prof. W.-C. Li
State Key Laboratory of Fine Chemicals
School of Chemical Engineering
Dalian University of Technology
Dalian 116024, P. R. China
Tel.:+86-411-84986355
Fax: +86-411-84986355
E-mail: wencuili@dlut.edu.cn

DOI: 10.1002/adma.201306273

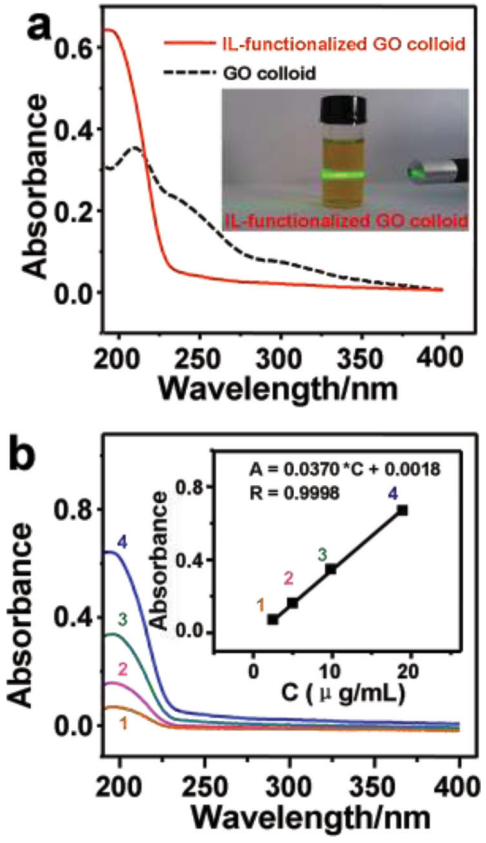

Figure 1. UV absorption spectra, (a) UV absorption spectra of pure GO colloid and IL-functionalized GO colloid. The inset shows the Tyndall effect of IL-functionalized GO colloid using a laser pointer. (b) UV absorption spectra of IL-functionalized GO colloid dispersed in an aqueous solution with different concentrations after storage for five months: (1) 2.34 μg mL^{-1}, (2) 4.68 μg mL^{-1}, (3) 9.36 μg mL^{-1}, (4) 18.7 μg mL^{-1}, the inset shows the dependence of the absorbance at 195 nm as a function of the concentration of IL-functionalized GO colloid.

two parts from the middle, implying that the NMCSs should have graphene as the inner layer with carbon coated on both its sides. No free carbon particles or naked graphene sheets are observed in FE-SEM images, suggesting perfect assembly of the reactants on the surface of GO sheets and the strong shape-directing effect of the GO sheets. As will be discussed later, the carbon sheet thickness is proportional to the R/GO ratio, we can deduce that the carbon layer should also be uniformly coated on graphene in the case of Figure 2a. Numerous open channels are seen between carbon sheets. These form a highly interconnected 3D porous structure, which is favorable for the access of electrolyte and minimizes transport distance between electrode and electrolyte. When the mass ratio of resorcinol to GO (R/GO) is fixed as 11.6, 32.1, 64.2, and 128.4, the respective average thicknesses of the carbon layer are measured to be 12 ± 2 nm (Figure 2a), 22 ± 2 nm (Figure 2b), 43 ± 2 nm (Figure 2c) and 85 ± 2 nm (Figure 2d). Further, the average thickness of the carbon layer is directly proportional to the mass ratio of R/GO and a high correlation coefficient of 0.9982 can be obtained (Figure 2e). This result enables one to continuously control the average thickness of the carbon layer over a wide range below 100 nm in a precise manner by simply adjusting the amount of reactants. An experiment with a R/GO value of 96.3 confirms the generality and prediction accuracy of the linearity (Figure 2f). However, when an exceedingly low dose of GO was used, e.g. the mass ratio of R/GO = 256.8, no sheet structures were obtained (Figure S3). In contrast, slight aggregation of NMCSs is visible when the mass ratio of R/GO was decreased to 5.80. It may be attributed to the van der Waals force between the very thin carbon sheets (Figure S4).

To compare the roles of different reagents, control experiments were performed in the absence of IL and GO. Without IL, the obtained carbon sheets stacked on each other and serious aggregation was observed (Figure S5), strongly suggesting the crucial role of IL as bridge molecules for the formation of uniform carbon coating layers. When no GO was used, large spherical units with an average diameter of 6±1 μm were seen (Figure S6), in turn demonstrating that the IL-functionalized GO sheets do direct the formation of the sheet structure.

Nitrogen sorption isotherms of NMCSs are plotted in **Figure 3**a and Figure S7. As shown, the typical type I isotherms confirm that NMCSs have a predominantly microporous structure and their specific surface areas are in the range 426 to 791 m^2 g^{-1} (Table S1). NMCSs-11.6 is discussed here as a typical example because it has the largest specific surface area. As shown in Figure 3a inset, the pore size distribution calculated by the NLDFT model shows that it has micropores of about 0.53 nm. Numerous large sheet structures and visible worm-like micropores in the carbon layer are also visible in a TEM image (Figure S8). The fact that there are no obvious lattice fringes indicates that NMCSs-11.6 is amorphous. In addition, as shown in Figure S9, the diagnostic peak assigned to GO at ca. 10° is absent in XRD patterns, which demonstrates that the original interlocked GO was reduced to graphene after pyrolysis and this graphene was integrated into the carbon matrix.[22] The reduced graphene oxide forms a high bulk conductive network in NMCSs-11.6 and its electrical conductivity is up to 5.82 S cm^{-1} at a low graphene content of 2.72 wt% (Table S1). The good conductivity enables the rapid movement of charge carriers through the graphene-centered thin carbon sheets. Furthermore, the broad reflection at 23° and a weaker one at 43° are characteristic of amorphous carbon.[45] The amorphous nature is also confirmed by the combination of a low intensity ratio of Raman peaks, I_G/I_D (0.49) and an observed negligible D+G band at ca. 2870 cm^{-1} and a 2D band at 2665 cm^{-1} from the Raman spectra as shown in Figure 3b and Figure S10. We carried out EDX mapping analysis and elemental analysis to prove the presence of nitrogen groups. As shown in Figure 3c, the EDX mapping images reveal a uniform distribution of nitrogen on carbon surface of NMCSs-11.6, suggesting homogeneous assembly of IL on the surface of GO. Elemental analysis reveals that the nitrogen content in NMCSs-11.6 is 0.62% (Table S1). In order to prove the improvement of the wettability of NMCSs-11.6, a contact angle test was performed to show that the contact angle is ~69°, demonstrating a hydrophilic surface (Figure 3c, inset). In addition, it is worth noting that a sample, which consists of only C, H and O shows hydrophobic properties as can be seen in Figure S11. On the basis of the information we have gathered,

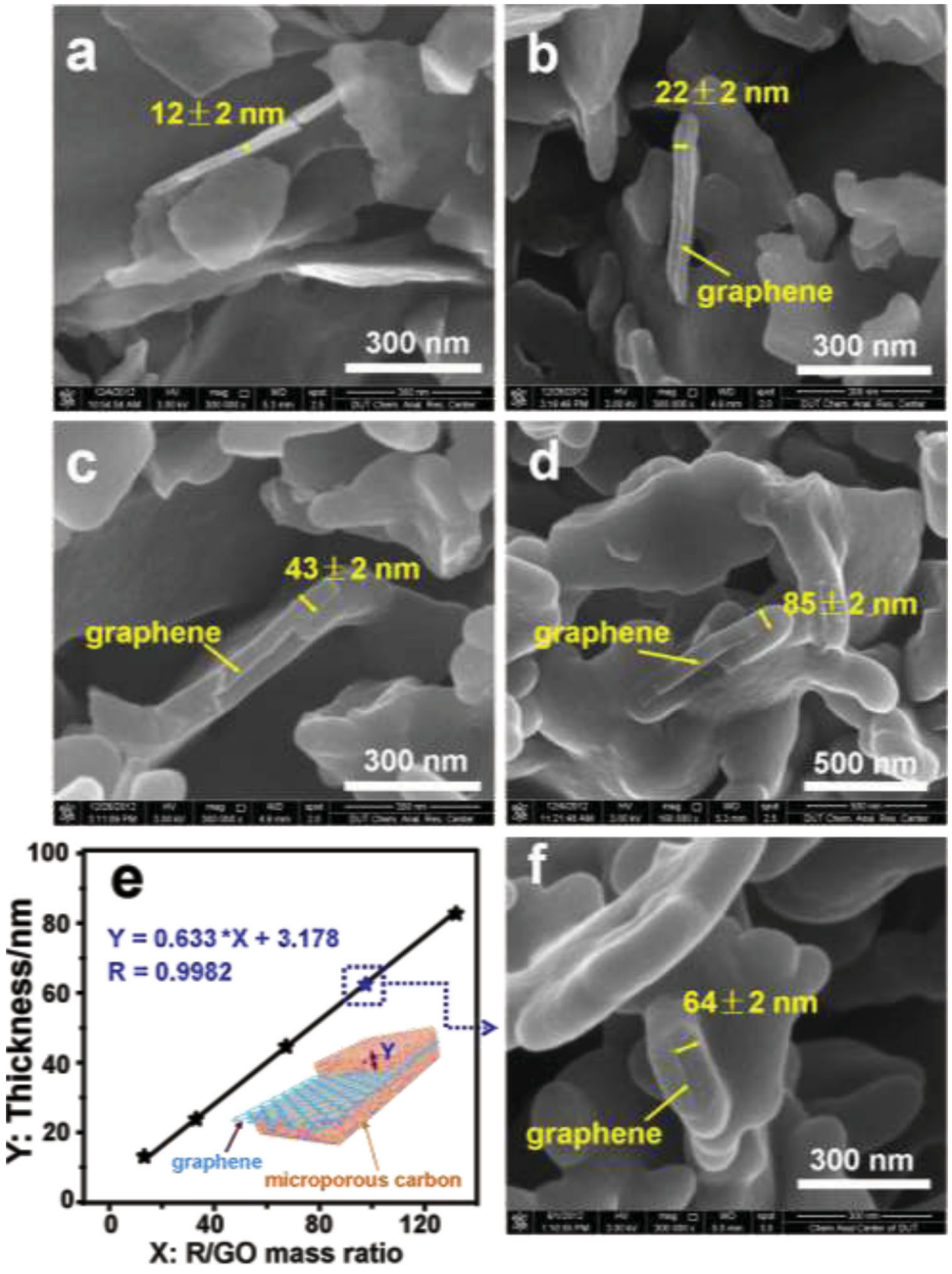

Figure 2. (a-d) FE-SEM images of NMCSs samples: (a) NMCSs-11.6, (b) NMCSs-32.1, (c) NMCSs-64.2, (d) NMCSs-128.4, the marked values shown are the average thickness of the carbon layer. (e) Linear relation between the average carbon layer thickness and the R/GO ratio. (f) FE-SEM image of an additional sample (NMCSs-96.3), which confirms the linear relationship in (e).

the nitrogen-doping has indeed altered the surface properties of NMCSs.

The above characterization results demonstrate the unique features of NMCSs-11.6, including abundant micropores, short diffusion paths, high electrically conductive networks and good wettability. Encouraged by these, a three-electrode system was used to evaluate the electrochemical properties of the NMCSs-11.6 for supercapacitors. As shown in **Figure 4**a–c and Figure S12, the cyclic voltammetry (CV) curves of NMCSs-11.6 have a rectangular-like shape even at a scan rate at 500 mV s^{-1} and the galvanostatic charge/discharge (GC) curves show no obvious ohmic drop even at a current density of 50 A g^{-1}, which indicates a favorable double layer energy storage behavior, low inner-pore ion-transport resistance and short diffusion distance during the charge-discharge process. Similar CV and GC curves were also achieved for other carbon samples, such as NMCSs-128.4 as shown in Figure S13. The specific capacitance of the NMCSs-11.6 is calculated to be 341 F g^{-1} at 5 mV s^{-1} and 213 F g^{-1} at 0.5 A g^{-1}. The capacitance retention ratio of NMCSs-11.6 was further evaluated

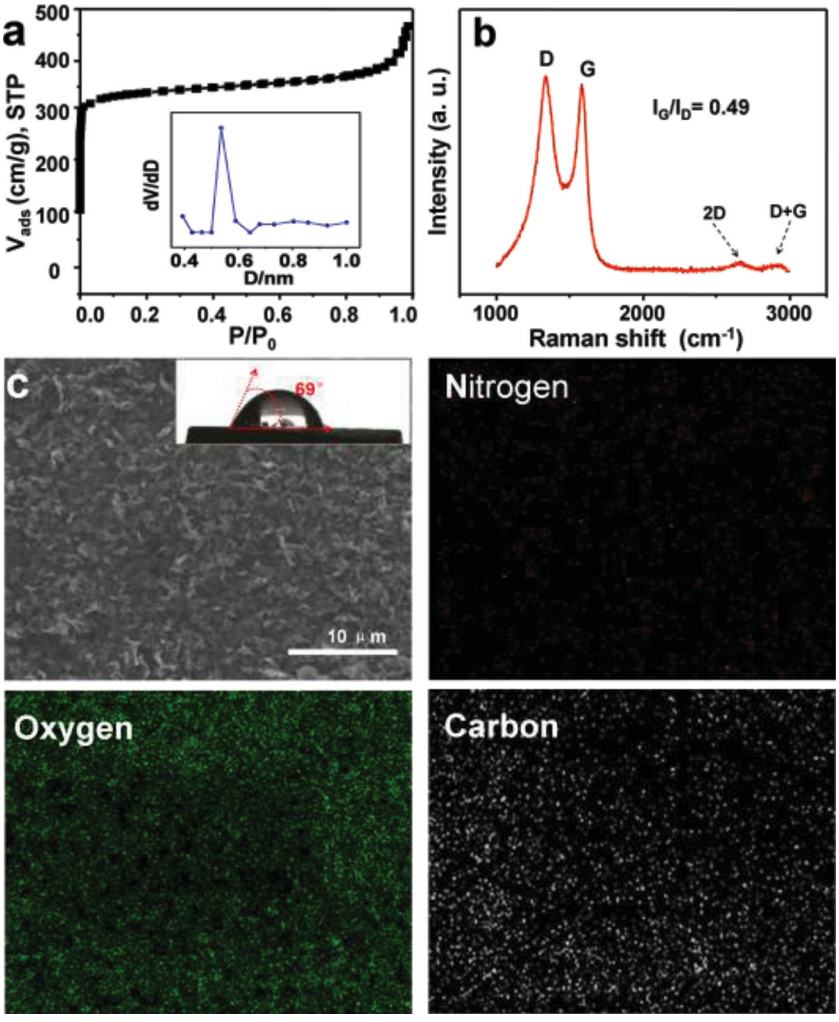

Figure 3. (a) Nitrogen sorption isotherm of NMCSs-11.6. The isotherm is vertically offset by 100 cm^3 g^{-1}, STP. The inset shows the pore size distribution below 1 nm calculated from the NLDFT model. (b) Raman spectrum of NMCSs-11.6. (c) EDX mapping images of C, O and N elements for NMCSs-11.6. The inset shows the contact angle test of NMCSs-11.6.

at various charge/discharge current densities. As shown in Figure 4d, a slight decrease in the capacitance retention ratio was observed when the current density was increased to 10 A g^{-1}, and a constant value of 75.1% (160 F g^{-1}) compared to the initial capacitance was maintained over a wide range of current density from 10 A g^{-1} to 50 A g^{-1}, highlighting an excellent suitability for high-rate operation. These results show that the NMCSs-11.6 electrode has advantages compared to other reported carbonaceous electrode materials in an aqueous electrolyte (Figure S14-15). Electrochemical impedance spectroscopy (EIS) was carried out to prove that the short diffusion path of NMCSs-11.6 for electrolyte ions enhances ion transport kinetics. As shown in Figure 4e, the nearly vertical line in the low frequency region indicates that the electrode shows an outstanding ion diffusion and migration behavior. In addition, the inconspicuous Warburg curve confirms the short ion diffusion path in the electrode.[46] We also consider that good wettability resulting from the N-doped polar surface also reduces ion-transport resistance in the solid-liquid interface.

The cycle life is an important requirement for supercapacitors and the capacitance retention as a function of cycle number is shown for NMCSs-11.6 in Figure 4f. The specific capacitance gradually increases in the first 2500 cycles, reaching 109.9% of the initial value, which may be associated with an activation process of the electrode material such as gradual wetting of the electrolyte deep inside the electrode.[47] A similar phenomenon has also been observed in other porous carbon electrodes.[48] Subsequently, the electrode shows a stable capacitance retention and retains 99.3% of its initial response after 35000 cycles at 1 A g^{-1}. Due to the improved wettability of the electrode, the shape of GC curves in the first ten cycles and last ten cycles are almost isosceles triangles.[49] Furthermore, the Ragone plot, which shows the relationship between energy density and power density per weight of active material, is another important way to evaluate the capacitive performance of an electrode.[14] As shown in Figure 4g, the energy and power density of the NMCSs-11.6 electrode were calculated as described in the electrode evaluation section (Supporting information). The maximum energy density of the electrode is 37.4 Wh kg^{-1}, while the highest power density (56.3 kW kg^{-1}) can reach the power target of the PNGV (Partnership for a new generation of vehicles),[23,50] thus supporting the applicability of the NMCSs-11.6-based supercapacitors as power-energy supply components. Furthermore, as provided in Figure 4g and Table S2, a careful comparison indicates that the NMCSs-11.6 is superior to, or at least comparable to many reported carbon-based supercapacitor electrode at high rates.[4,51] These electrochemical results strongly suggest the critical importance to obtain high rate and long cycle life supercapacitors of integrating high microporosity with narrow pores for charge storage, a N-doped surface for wettability, and short diffusion paths for ion transport in the conductive carbon sheets.

In summary, from a synthesis perspective, 2D nitrogen-doped microporous carbon sheets were prepared by an ionic liquid-assisted, simple and controllable method. The resulting NMCSs show a sheet structure associated with graphene as an inner layer with a microporous carbon coating on both sides. The thickness of the microporous carbon layer can be precisely controlled over a wide range below 100 nm by simply changing the ratio of reactants to GO content. The NMCSs show abundant micropores with narrow pores, short diffusion paths, high electrical conductive networks and good wettability. When used as the electrode for supercapacitors,

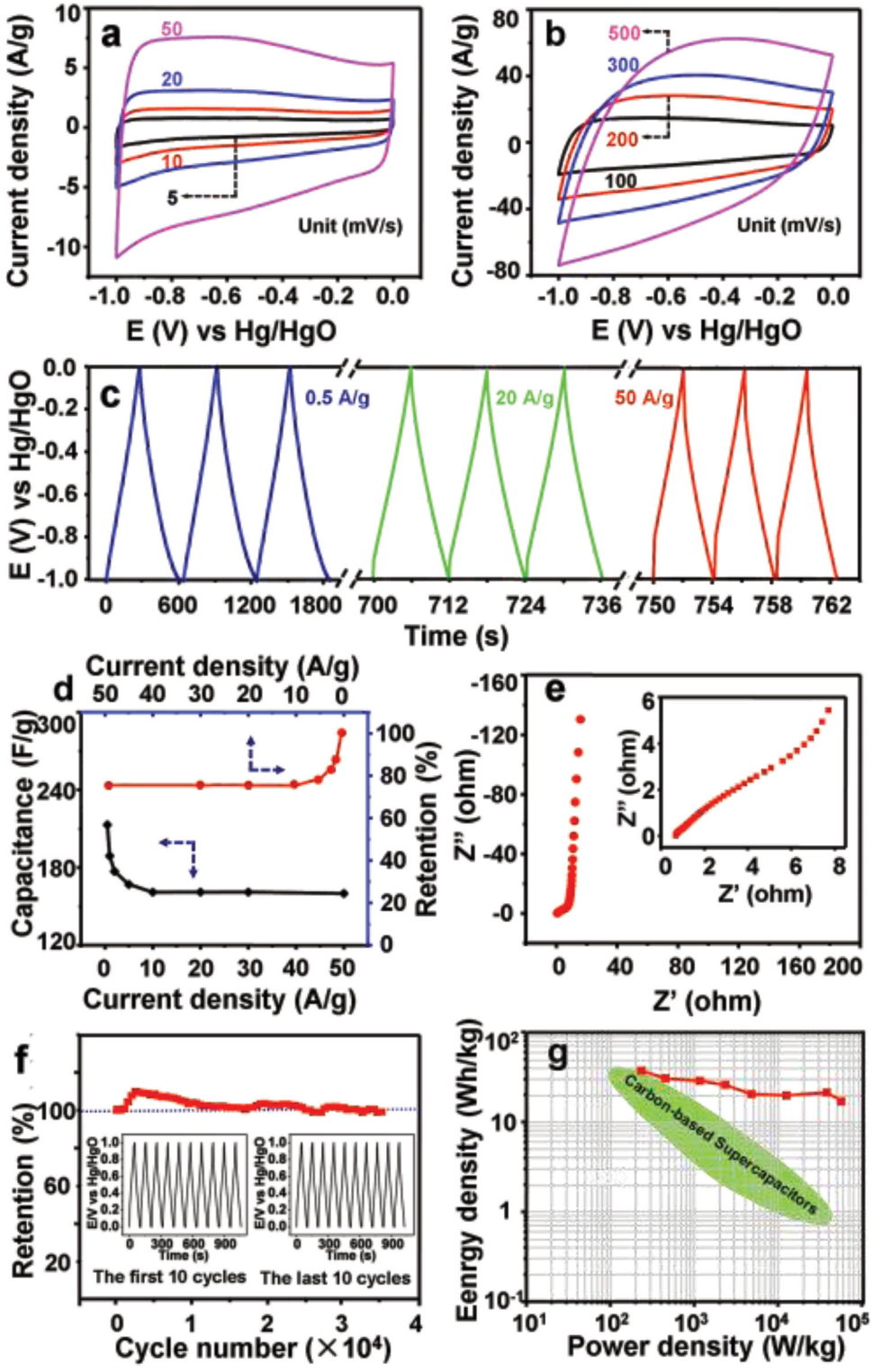

Figure 4. Electrochemical performance of NMCSs-11.6. (a and b) CV curves at different scan rates. (c) GC curves at different current densities. (d) Specific capacitance and its retention ratio at different current densities. (e) Nyquist plots with a magnification for the high-frequency region in the inset. (f) Cycle life test with a two-electrode setup at 1.0 A g^{-1}. The first and last ten cycles of GC curves are also shown in the inset. (g) Ragone plots.

the NMCSs show excellent rate capability, good long-term stability, high specific capacitance and high energy/power density. Optimistically, our synthesis strategy may open a window for the novel design of nanostructure that has several advantages for use as a high-performance supercapacitor electrode.

Supporting Information

Supporting Information is available from the Wiley Online Library or from the author.

Acknowledgements

The project was supported by the National Natural Science Funds (No. 21376047), National Program on Key Basic Research Project of the Ministry of Science and Technology (No. 2013CB934104) and National Science Fund for Distinguished Young Scholars (No. 21225312).

Received: December 24, 2013
Revised: January 29, 2014
Published online: March 20, 2014

[1] H. Nishihara, T. Kyotani, *Adv. Mater.* **2012**, *24*, 4473.
[2] L. L. Zhang, X. S. Zhao, *Chem. Soc. Rev.* **2009**, *38*, 2520.
[3] J. R. Miller, P. Simon, *Science* **2008**, *321*, 651.
[4] Y. Zhai, Y. Dou, D. Zhao, P. F. Fulvio, R. T. Mayes, S. Dai, *Adv. Mater.* **2011**, *23*, 4828.
[5] D Carriazo, F Picó, M. C. Gutiérrez, F. Rubio, J. M. Rojo, F. del Monte, *J. Mater. Chem.* **2010**, *20*, 773.
[6] G. Hasegawa, M. Aoki, K. Kanamori, K. Nakanishi, T. Hanada, K. Tadanaga, *J. Mater. Chem.* **2011**, *21*, 2060.
[7] W. R. Li, D. H. Chen, Z. Li, Y. F. Shi, Y. Wan, J. J. Huang, J. J. Yang, D. Y. Zhao, Z. Y. Jiang, *Electrochem. Commun.* **2007**, *9*, 569.
[8] C. Kim, Y. O. Choi, W. J. Lee, K. S. Yang, *Electrochim . Acta* **2004**, *50*, 883.
[9] X. Q. Zhang, Q. Sun, W. Dong, D. Li, A. H. Lu, J. Q. Mu, W. C. Li, *J. Mater. Chem.* **2013**, *1*, 9449.
[10] L. Hu, M. Past, F. L. Mantia, L. F. Cui, S. Jeong, H. D. Deshazer, Y. Cui, *Nano Lett.* **2010**, *10*, 708.
[11] Z. S. Wu, Y. Sun, Y. Z. Tan, S. Yang, X. Feng, K. Müllen, *J. Am. Chem. Soc.* **2012**, *134*, 19532.
[12] D. W. Wang, F. Li, J. Zhao, W. Ren, Z. G. Chen, J. Tan, Z. S. Wu, I. Gentle, G. Q. Lu, H. M. Cheng, *ACS Nano* **2009**, *3*, 1745.
[13] Q. Wu, Y. Xu, Z. Yao, A. Liu, G. Shi, *ACS Nano* **2010**, *4*, 1963.
[14] C. Liu, Z. Yu, D. Neff, A. Zhamu, B. Z. Jang, *Nano Lett.* **2010**, *10*, 4863.
[15] X. Yang, C. Cheng, Y. Wang, L. Qiu, D. Li, *Science* **2013**, *341*, 534.
[16] Y. Zhu, S. Murali, M. D. Stoller, K. J. Ganesh, W. Cai, P. J. Ferreira, A. Pirkle, R. M. Wallace, K. A. Cychosz, M. Thommes, D. Su, E. A. Stac, R. S. Ruoff, *Science* **2011**, *332*, 1537.
[17] L. L. Zhang, X. Zhao, M. D. Stoller, Y. Zhu, H. Ji, S. Murali, Y. Wu, S. Perales, B. Clevenger, R. S. Ruoff, *Nano Lett.* **2012**, *12*, 1806.
[18] H. Ji, Y. Mei, O. G. Schmidt, *Chem. Commun.* **2010**, *46*, 3881.
[19] J. Mi, X. R. Wang, R. J. Fan, W. H. Qu, W. C. Li, *Energy Fuels* **2012**, *26*, 5321.
[20] J. Chmiola, G. Yushin, Y. Gogotsi, C. Portet, P. Simon, P. L. Taberna, *Science* **2006**, *313*, 1760.
[21] J. S. Huang, B. G. Sumpter, V. Meunier, *Angew. Chem. Int. Ed.* **2008**, *47*, 520.
[22] G. P. Hao, A. H. Lu, W. Dong, Z. Y. Jin, X. Q. Zhang, J. T. Zhang, W. C. Li, *Adv. Energy Mater.* **2013**, *6*, 3740.
[23] D. W. Wang, F. Li, M. Liu, G. Q. Lu, H. M. Cheng, *Angew. Chem. Int. Ed.* **2008**, *47*, 373.
[24] M. Endo, Y. J. Kim, H. Ohta, I. T. Inoue, T. Hayashi, Y. Nishimura, T. Maeda, M. S. Dresselhaus, *Carbon* **2002**, *40*, 2613.
[25] L. Qie, W. Chen, H. Xu, X. Xiong, Y. Jiang, Y. Jiang, X. Hu, Y. Xin, Z. Zhang, Y. Huang, *Energy Environ. Sci.* **2013**, *6*, 2497.
[26] S. Yoon, S. M. Oh, C. W. Lee, J. H. Ryu, *J. Electroanal. Chem.* **2011**, *650*, 187.
[27] M. Z. Bazant, B. D. Storey, A. A. Kornyshev, *Phys. Rev. Lett.* **2011**, *106*, 046102.
[28] F. Liu, S. Song, D. Xue, H. Zhang, *Adv. Mater.* **2012**, *24*, 1089.
[29] L. Wang, L. Sun, C. Tian, T. Tan, G. Mu, H. Zhang, H. Fu, *RSC Adv.* **2012**, *2*, 8359.
[30] J. Wei, D. Zhou, Z. Sun, Y. Deng, Y. Xia, D. Zhao, *Adv. Funct. Mater.* **2012**, *23*, 2322.
[31] D. C. Guo, J. Mi, G. P. Hao, W. Dong, G. Xiong, W. C. Li, A. H. Lu, *Energy Environ. Sci.* **2013**, *6*, 652.
[32] Z. Wen, X. Wang, S. Mao, Z. Bo, H. Kim, S. Cui, G. Lu, X. Feng, J. Chen, *Adv. Mater.* **2012**, *24*, 5610.
[33] M. Zhou, X. Li, J. Cui, T. Liu, T. Cai, H. Zhang, S. Guan, *Int. J. Electrochem. Sci.* **2012**, *7*, 9984.
[34] A. Heintz, *J. Chem. Thermodyn.* **2005**, *37*, 525.
[35] Z. Ma, J. H. Yu, S. Dai, *Adv. Mater.* **2010**, *22*, 261.
[36] J. S. Lee, X. Wang, H. Luo, G. A. Baker, S. Dai, *J. Am. Chem. Soc.* **2009**, *131*, 4596.
[37] J. S. Lee, X. Wang, H. Luo, S. Dai, *Adv. Mater.* **2010**, *22*, 1004.
[38] W. Yang, T. P. Fellinger, M. Antonietti, *J. Am. Chem. Soc.* **2011**, *133*, 206.
[39] J. P. Paraknowitsch, J. Zhang, D. Su, A. Thomas, M. Antonietti, *Adv. Mater.* **2010**, *22*, 87.
[40] P. Zhang, J. Yuan, T. P. Fellinger, M. Antonietti, H. Li, Y. Wang, *Angew. Chem. Int. Ed.* **2013**, *52*, 6028.
[41] T. Qian, C. Yu, S. Wu, J. Shen, *J. Mater. Chem. A.* **2013**, *1*, 6539.
[42] Y. Fu, J. Zhang, H. Liu, W. C. Hiscox, Y. Gu, *J. Mater. Chem. A.* **2013**, *1*, 2663.
[43] X. S. Zhou, T. B. Wu, B. J. Hu, G. Y. Yang, B. X. Han, *Chem. Commun.* **2010**, *46*, 3663.
[44] J. Lu, J. X. Yang, J. Wang, A. Lim, S. Wang, K. P. Loh, *ACS Nano* **2009**, *3*, 2367.
[45] L. Lu, V. Sahajwalla, C. Kong, D. Harris, *Carbon* **2001**, *39*, 1821.
[46] Y. Wang, Z. Q. Shi, Y. Huang, Y. F. Ma, C. Y. Wang, M. M. Chen, Y. S. Chen, *J. Phys. Chem. C* **2009**, *113*, 13103.
[47] J. Yan, P. Liu, Z. J. Fan, T. Wei, L. J. Zhang, *Carbon* **2012**, *50*, 2179.
[48] Y. Yoon, K. Lee, C. Baik, H. Yoo, M. Min, Y. Park, S. M. Lee, H. Lee, *Adv. Mater.* **2013**, *25*, 4437.
[49] Y. Chen, X. Zhang, D. Zhang, P. Yu, Y. Ma, *Carbon* **2011**, *49*, 573.
[50] N. S. Choi, Z. Chen, S. A. Freunberger, X. Ji, Y. K. Sun, K. Amine, G. Yushin, L. F. Nazar, J. Cho, P. G. Bruce, *Angew. Chem. Int. Ed.* **2012**, *51*, 9994.
[51] Y. Gogotsi, P. Simon, *Science* **2011**, *334*, 917.